Supporting Information

Leaf-inspired nanofibrous mat-based composite for liquid-gas phase change-driven dynamic adaptive electromagnetic interference shielding

Junqing Shi, Jialong Tian, Yimei Xu, Fenglin Huang, Qufu Wei, Yibing Cai*

College of Textile Science and Engineering, Jiangnan University, Wuxi, Jiangsu 214122, the People's Republic of China

Corresponding author: Yibing Cai

E-mail address: yibingcai@jiangnan.edu.cn

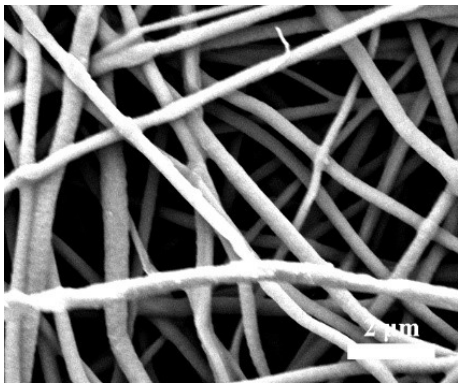

Fig. S1 SEM image of PP.

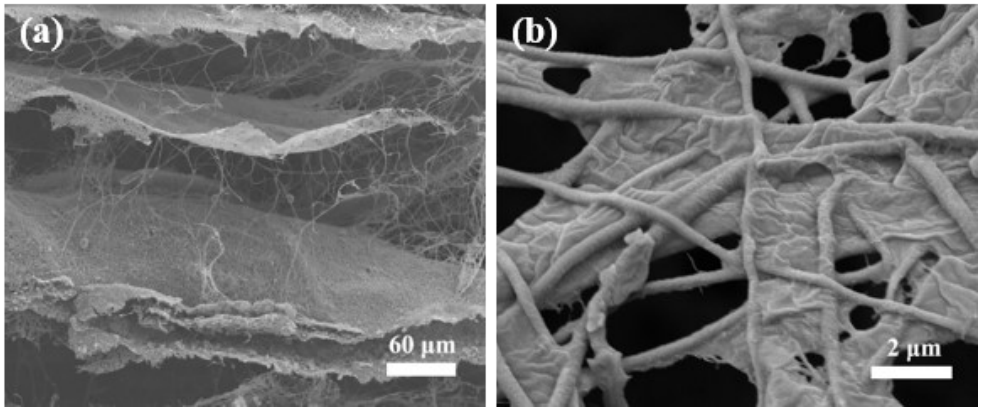

Fig. S2 SEM image of PA.

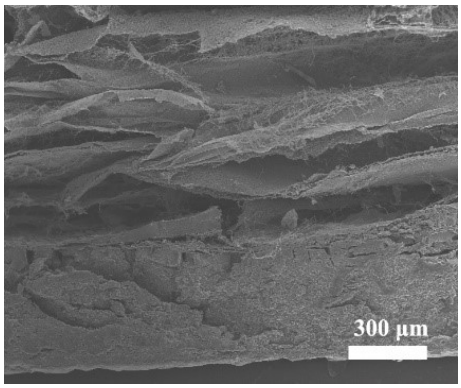

Fig. S3 SEM image of the connection interface between PA and PF.

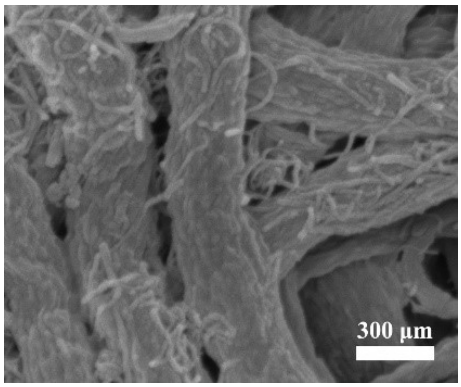

Fig. S4 SEM image of PF layer.

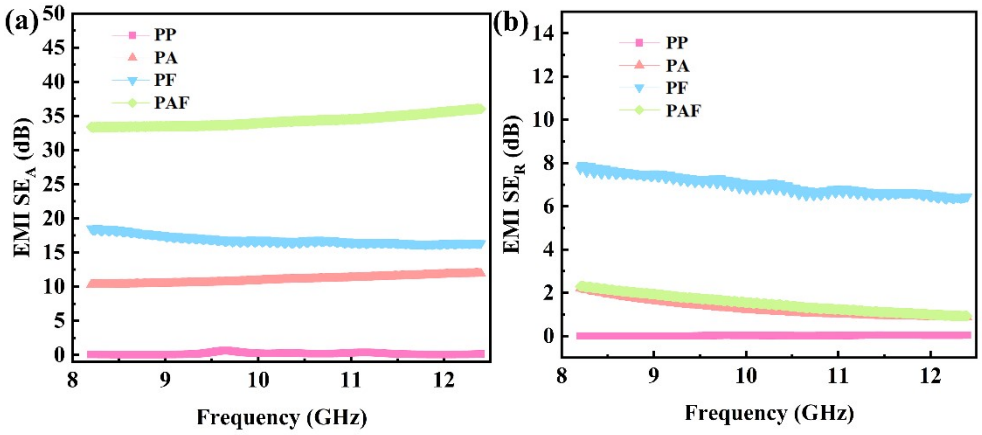

Fig. S5 SE_A and SE_R values of PP, PA, PF and PAF.

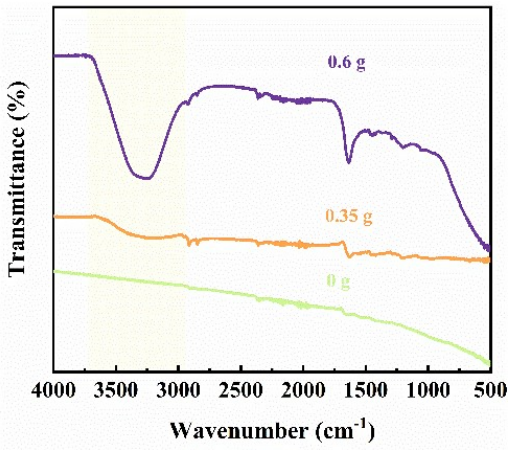

Fig. S6 FTIR spectra of PAF after introducing different amounts of water.

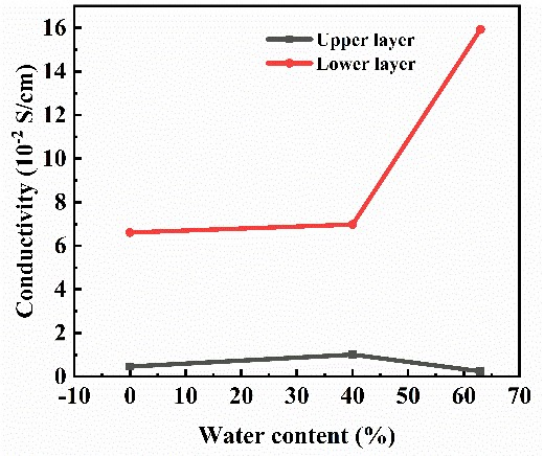

Fig. S7 Electrical conductivity of upper and lower layer of PAF with different water contents.

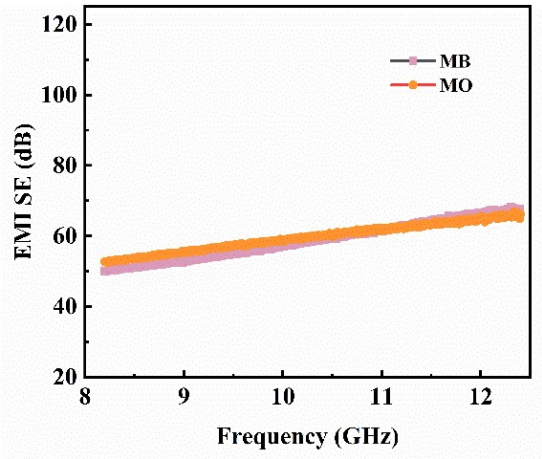

Fig. S8 EMI SE values of PAF after adsorbing simulated wastewater (MB and MO).

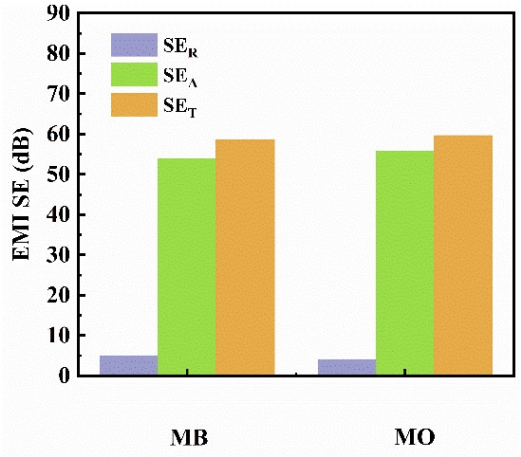

Fig. S9 SE_R, SE_A, SE_T of PAF after adsorbing simulated wastewater (MB and MO).

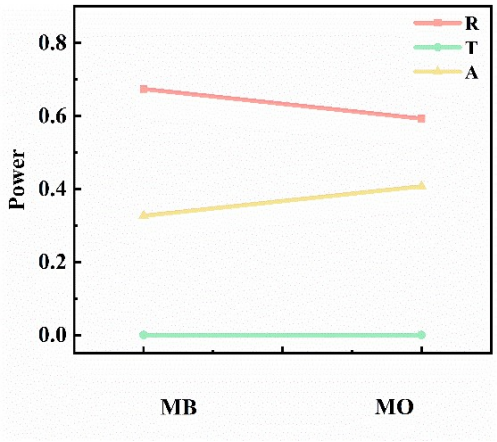

Fig. S10 R, A, and T power coefficients of PAF after adsorbing simulated wastewater (MB and MO).

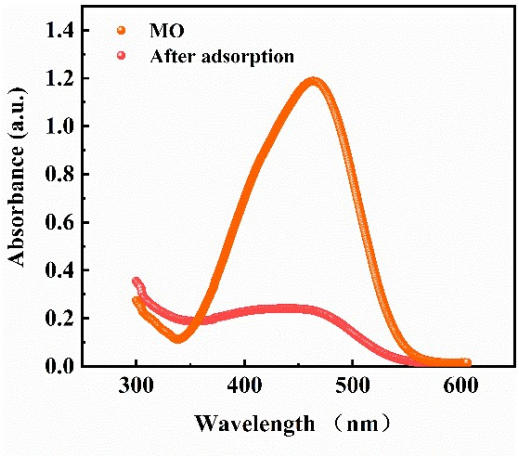

Fig. S11 Absorbance of PAF adsorbing MB.

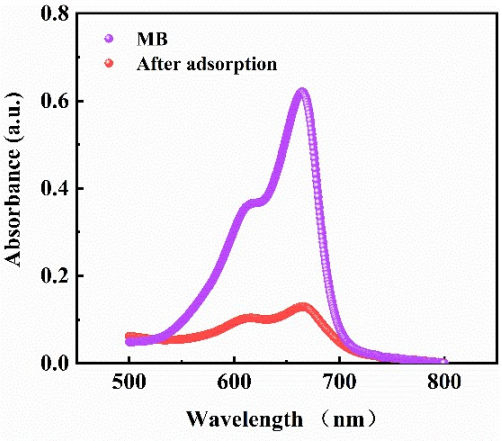

Fig. S12 Absorbance of PAF adsorbing MO.

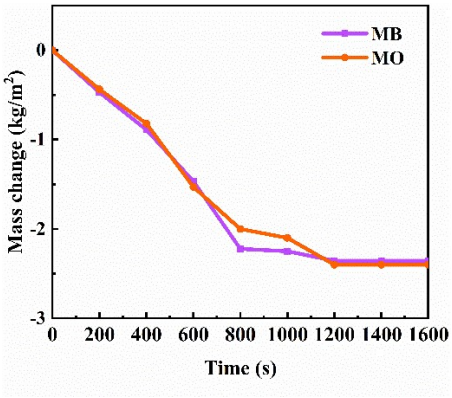

Fig. S13 Mass change-time curves of water evaporation per unit area of PAF after adsorbing MB and MO.

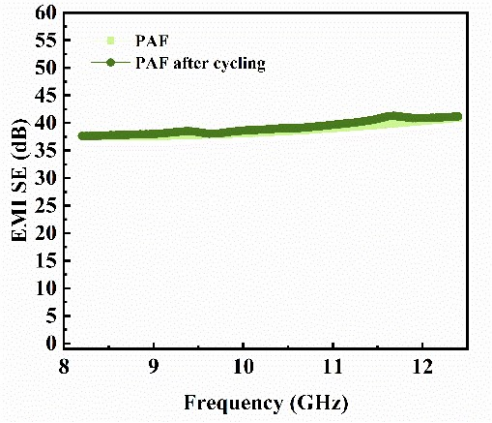

Fig. S14 EMI SE values of PAF before and after cycling.

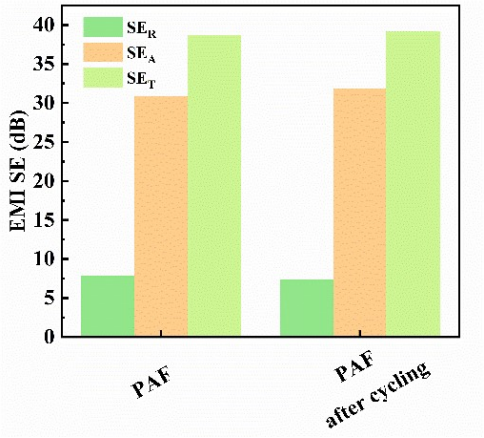

Fig. S15 SE_R, SE_A, SE_T of PAF before and after cycling.

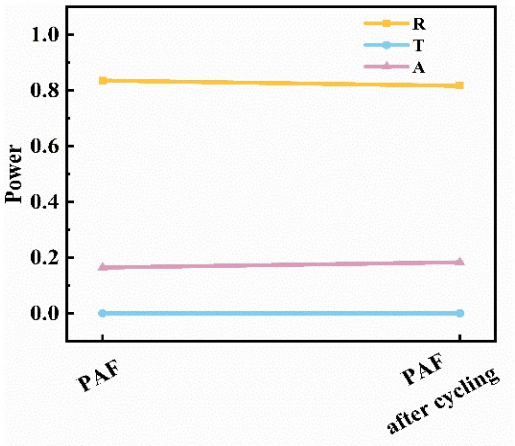

Fig. S16 R, A, and T power coefficients of PAF before and after cycling.

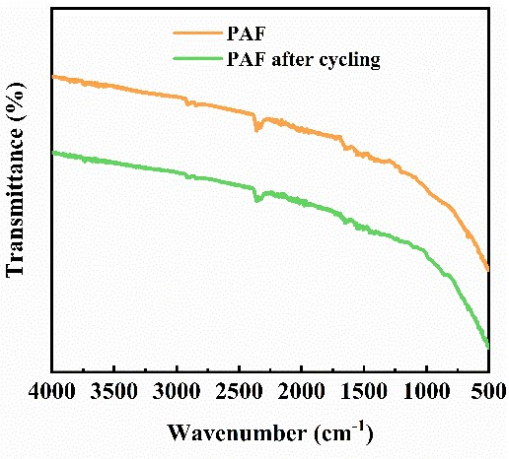

Fig. S17 FTIR spectra of PAF before and after cycling.

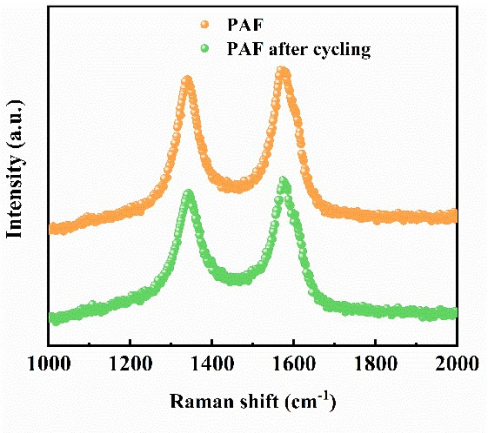

Fig. S18 Raman spectra of PAF before and after cycling.

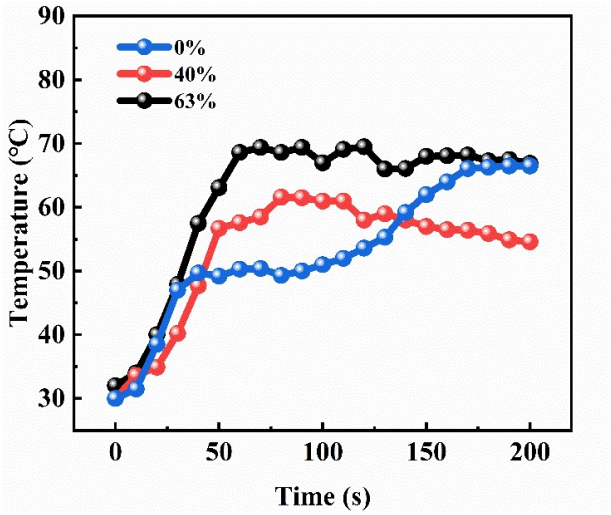

Fig. S19 Thermal radiation temperature evolution of PAF with 0, 40 and 63 % water contents during heating (on a 150 °C hot plate).

Table S1. Comparison of EMI SE and absorption power coefficient at X-band of fabricated PAF with those of other EMI shielding composites in literature.

Samples	EMI SE (dB)	Absorption Power Coefficient (A)	Refs
Emulsion-based Graphene Aerogels	23.4	0.63	[1]
PVDF-PEDOT NFs	50	0.68	[12]
AgNW@MXene/Wood	44.96	0.36	[16]
MXene/Fe_3O_4@aMWCNT	51.6	0.31	[21]
Carbon Fiber/Bi_2Te_3	45	0.03	[47]
Multi-walled Carbon Nanotubes/Poly(ε-caprolactone)	40.9	0.1	[48]
TPU/PDA/CNT	48.3	0.19	[49]
CF-NiCo Composite	53	0.15	[50]
TPU/PDMS/AgNW/MXene	41.7	0.043	[51]
Leather/MXene/Shear Stiffening Gel/Nonwoven Fabrics	40	0.1	[52]
Ag-NPs@CNT/PDA@CNT/Fabric	35.3	0.07	[53]
TPAE@Ti_3C_2Tx	44	0.7	[54]
MWCNTs/CNF-Pluronic F127/BPA-PEN	26.7	0.52	[55]
PAF Composite	35.9 (Min) 64.4 (Max)	0.71 0.31	This work

In order to adapt to more complex environments so as to improve the environmental adaptability of the materials, the EMI shielding performance of PAF after adsorbing wastewater (MB, MO) was tested. As shown in Fig. S8 and S9, the EMI SE values after adsorbing MB and MO reach 58.6 dB and 59.6 dB, respectively, which are higher than the SE value of 51.9 dB for pure water. As shown in Fig. S10, the power coefficients of PAF after adsorbing MB and MO are calculated, and the absorption power coefficients are 0.33 and 0.41, respectively, which are lower than that of pure water with 0.62. This is attributed to the fact that the molecular MB and MO have more free ions in the water, which promotes electron transfer and reflection loss of PAF. Notably, PAF also possesses good adsorption capacity on MB (solution concentration 3.5 mg/L) and MO (solution concentration 15 mg/L). As shown in Fig. S11 and S12, the adsorption rates of PAF on MB (464 nm) and MO (664 nm) after 12 h are 78.9 % and 79.2 %, respectively. This is due to porous structure of PAF providing more active sites for adsorption of dye molecules. As shown in Fig. S13, during simulated transpiration, it can be seen that the evaporation within 1200 s was 2.3 kg/m^2 and 2.4 kg/m^2, respectively.